PHYSICAL REVIEW C **74**, 011302(R) (2006)

Calculating the nuclear mass in the very high angular momentum regime

B. G. Carlsson and I. Ragnarsson
Division of Mathematical Physics, LTH, Lund University, Post Office Box 118, SE-221 00 Lund, Sweden
(Received 24 March 2005; published 27 July 2006)

Macroscopic-microscopic methods are applied in the high-spin regime to calculate the nuclear binding energy ("mass") as a function of proton number, neutron number, and angular momentum. Masses at high spin are calculated using the cranked Nilsson-Strutinsky model together with two different liquid drop models, the Lublin-Strasbourg drop model and the finite range liquid drop model. When comparisons are made with experimental data, a similar agreement between theory and experiment is obtained as for ground-state masses.

DOI: 10.1103/PhysRevC.74.011302 PACS number(s): 21.10.Dr, 21.10.Re, 21.60.Ev

A fundamental property of nuclei is their mass or, equivalently, their binding energy $\mathcal{B}$. The variation of the nuclear mass with proton and neutron number will reveal the shell effects, which are closely related to the magic numbers and the extra binding associated with these numbers. It will also give some general idea about which regions of nuclei are deformed and whether some specific particle numbers give rise to extra binding for deformed nuclear shapes.

In recent years, it has become possible to study a large number of nuclei up to very high angular momenta. A natural extension is then to study the variation of the total nuclear energy as a function of the angular momentum I, that is, to extend the investigations of the binding energy to three dimensions, $\mathcal{B}(Z, N, I)$. Such studies were applied to relatively low spin states long ago [1] when especially so-called backbending plots in gauge space were considered. Thus, from differences in the binding energy taken at constant spin I, it was possible to conclude for example that the borders between spherical and deformed nuclei depend on the particle number. More recently, the total binding energy of the highly deformed bands in Nd isotopes has been used to learn about the pairing gap at high spins [2].

The absolute energy can in principle be calculated in standard high-spin calculations based on the cranking model. However, to our knowledge, only some preliminary comparisons between experiment and macroscopic rotating liquid drop energies have been presented [3,4], but no attempts have been made to describe the binding energy of high-spin states in full calculations including the shell energy (or in cranked Hartree-Fock or relativistic mean-field calculations). Therefore, it is our purpose to introduce such calculations, based on the rotating liquid drop + shell correction energies. They will be applied to a representative selection of nuclei with mass numbers in the range $A \approx 20-200$, whose level schemes are known up into the unpaired regime and which have been successfully interpreted in calculations.

In experimental studies of high-spin spectra, the natural quantity to consider is of course the excitation energy relative to the ground state. This is also a relevant quantity when describing the structure of low- and intermediate-spin states formed at similar deformations as the ground state. Going to higher spins, however, quite different deformations or coupling schemes might develop and to learn about the structure in this spin regime, the measured excitation energy is no longer useful, because it will depend as strongly on the (unrelated) low-spin properties, where large shell effects are often seen, as on the high-spin properties. Therefore, for systematic studies over all spin values and especially in the high-spin regime, it appears necessary to use a reference not dependent on the ground-state mass. A natural choice is then the absolute binding energy $\mathcal{B}(Z, N, I)$.

In the macroscopic-microscopic approach (see, e.g., Ref. [5]), the total nuclear energy is calculated as the sum of the liquid drop energy $E_{\rm ld}$, the shell correction energy $E_{\rm shell}$, and the pairing correction energy $\delta E_{\rm pair} = E_{\rm pair} - \langle E_{\rm pair}\rangle$. The ground-state energy is then obtained as the minimum over deformation of this sum, that is,

$$E_{\rm tot}(Z, N) = \min_{\varepsilon_i} [E_{\rm ld}(Z, N, \varepsilon_i) + E_{\rm shell}(Z, N, \varepsilon_i) + \delta E_{\rm pair}(Z, N, \varepsilon_i)], \quad (1)$$

where ε_i indicates the deformation coordinates. This formula can be generalized to include angular momentum I by using the principal-axis cranking model and the shell-correction method at high angular momenta (see, e.g., Ref. [6]). In a first step this is done only for high-spin states where pairing can be neglected.

In analogy with Eq. (1) the total energy at spin I is then obtained as

$$E_{\rm tot}(Z, N, I) = \min_{\varepsilon_i} [E_{\rm rld}(Z, N, I, \varepsilon_i) + E_{\rm shell}(Z, N, I, \varepsilon_i)]. \quad (2)$$

The smoothly varying energy $E_{\rm rld}$ is the rotating liquid drop energy, which is assumed to be of standard form [6],

$$E_{\rm rld}(Z, N, I, \varepsilon_i) = E_{\rm ld}(Z, N, \varepsilon_i) + \frac{\hbar^2 I(I+1)}{2\mathcal{J}_{\rm rig.}(Z, N, \varepsilon_i)}, \quad (3)$$

where $E_{\rm ld}$ is the static liquid drop energy and $\mathcal{J}_{\rm rig.}$ is the rigid-body moment of inertia. The shell energy is evaluated from the energy eigenvalues of the cranked single-particle Hamiltonian, $h^\omega = h - \omega j_x$, where, for each angular momentum I (and each many-body configuration), the rotational frequency is chosen to give the correct I value, where I is defined as the sum of the expectation values of j_x [7].

Although nuclear ground-state masses have mainly been calculated using the folded-Yukawa potential [5], we will use the modified oscillator potential for the present application,

because it is only in this model (referred to as cranked Nilsson-Strutinsky (CNS) [7,8]) that systematic high-spin calculations have been carried out for nuclei in essentially all mass regions. The main advantage of this model is the unique possibilities to fix configurations in the high-spin regime and follow their evolution in deformation space $(\varepsilon_2, \varepsilon_4, \gamma)$ as spin increases. This in turn relies on the use of a rotating harmonic oscillator basis, making it possible to treat the main oscillator quantum number in this basis as pure.

All kinds of different bands have been observed in the very high spin regime. Although the deformation of superdeformed or highly deformed bands is in general very stable, most bands at normal deformation show tendencies to terminate at very high spins, thus changing their deformation in the direction toward rotation around the symmetry axis ($\gamma = 60^\circ$) or in many cases even terminating in a noncollective aligned state. Since the model treats states of single-particle character on the same footing as collective states, it is well suited for describing such a transition [7,8]. As concluded in a recent review [9], the model "appears to be extremely successful in the identification and classification of such terminating bands, producing results that are in very good quantitative agreement with data." It is only for heavy nuclei (i.e., mainly in the rare-earth region) that normal-deformed bands do not show any noticeable tendencies to terminate even at the highest spin values observed. As exemplified for ^{162}Er [10] in the following, our model is also well suited for describing such bands. One could also note that many of the basic ideas for the interpretation of superdeformed (SD) bands have been introduced using the CNS model (see, e.g., Refs. [9,11]).

To keep the number of parameters as small as possible, we have used the so-called $A = 110$ parameters [7] for all nuclei. These parameters have been optimized for nuclei with $A = 100$–150 but should be approximately applicable for all mass numbers.

For the static liquid drop energy $E_{\rm ld}$ [see Eq. (3)], we will consider two different macroscopic models that have recently been applied to large-scale mass calculations, namely the finite range liquid drop model (FRLDM) [5] and the Lublin-Strasbourg drop (LSD) model [12]. The latter is a recent version of the classical Myers-Swiatecki expressions [13], where an $A^{1/3}$ curvature term has been added. Both these models have been fitted to the known masses for $Z, N \geqslant 8$ nuclei, giving rms errors in the range 0.6–0.8 MeV, with a somewhat better accuracy for the LSD model, where empirical [13] instead of microscopic shell corrections have been used for $Z, N \leqslant 28$.

Comparing Eqs. (1) and (2), we note that we should remove $\langle E_{\rm pair}\rangle$ in the liquid drop energy if it is assumed that the full pairing energy, $E_{\rm pair} = \langle E_{\rm pair}\rangle + \delta E_{\rm pair}$, is negligible at high spin. Furthermore, in the FRLDM fit, a zero-point energy for vibrations in the elongation direction is included. A new fit to ground-state masses using the FRLDM was therefore performed with $\langle E_{\rm pair}\rangle$ removed from the macroscopic energy and with no explicit zero-point energy. The rms error of the new fit is essentially the same as in the old fit. With this in mind we will not include any explicit zero-point energy in the present applications. This is also based on the fact that most states are triaxial at high spin (cf. Fig. 4), indicating that it would be inconsistent to correct only for vibrations in the elongation direction. At spherical shape the difference between the old and the new fit is a smooth analytic function in Z and N and because the LSD fit is based on the FRLDM fit, it is compensated by the same function.

The average moment of inertia $\mathcal{J}_{\rm rig.}$ [see Eq. (3)] is calculated for rotation around a principal axis for a rigid body with a radius parameter r_0 and a diffuse surface introduced in the form of a Yukawa folding function with range a [14]. The parameters r_0 and a are obtained by a fit to experimentally determined nuclear charge density distributions. We fit the rms value of the radius $\langle r^2\rangle^{1/2}(\varepsilon_2, r_0, a)$ to the values given in Ref. [15] for 116 nuclei with $A > 16$. The quadrupole deformations of the ground states are taken from Ref. [5]. The result of the fit is $r_0 = 1.1599$ fm and $a = 0.5984$ fm and the standard deviation of the errors is $s = 0.0454$ fm.

Figure 1 illustrates the total energy for a few nuclei as a function of spin. It is drawn using the LSD model for the static liquid drop energies and radius constants $r_0 = 1.16$ fm and $a = 0.6$ fm obtained from the fit just described. For each nucleus the energy of the corresponding rotating liquid drop has been subtracted. This is a straightforward generalization of "standard" mass plots (e.g., Figs. 1 and 2 of Ref. [5]), which gives a convenient scaling when comparing the microscopic energy for different nuclei or when comparing theory and experiment. Low values indicate that states are built at a relatively low energy cost, arising from a reduced level density around the Fermi surface.

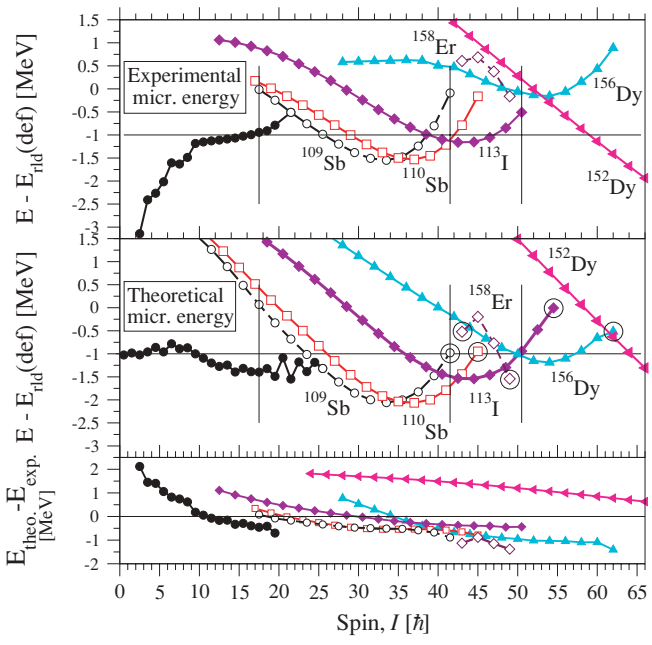

FIG. 1. (Color online) Experimental (top panel) and theoretical (middle panel) microscopic energies and their difference (lower panel) for some well-established high-spin bands in $A = 109$–158 nuclei. The LSD model and a diffuse surface ($r_0 = 1.16$ fm, $a = 0.6$ fm) has been used when calculating the first and second terms, respectively, of Eq. (3). Calculated states where all valence nucleons have their spin vectors aligned with the axis of rotation (terminating states) are encircled.

The yrast line for ^{109}Sb [7] in Fig. 1 is drawn starting from low spins where the difference between calculations and experiment should be an approximate measure of the pairing energy, which is not included in the calculations. The high-spin bands in ^{109,110}Sb are observed to termination at $I = 41.5$ and $I = 45$, respectively [7]. The configuration assignment for the ^{109}Sb band is supported by unpaired cranked relativistic mean-field (CRMF) calculations [16], where, however, it was only possible to follow the band to the $I = 39.5$ state. The energy curves in Fig. 1 reveal that the observed and calculated differences relative to the rotating liquid drop energy are essentially identical for the two bands in ^{109}Sb and ^{110}Sb. This is a strong indication that the energy of the neutron $h_{11/2}$ orbital, which is filled in ^{110}Sb and empty in ^{109}Sb, is properly described in the calculations. The band in ^{113}I (band 1 of Ref. [17]) has a higher terminating spin value at $I^{\pi} = 54.5^{+}$ and is observed up to $I = 50.5$. The favored terminations in ^{158}Er at $I^{\pi} = 43^{-}, 49^{-}$ [18] show more typical single-particle features than the unfavored terminations in, for example, ^{109,110}Sb. The ^{156}Dy band [19], which is yrast only at the highest spin values, is observed to a tentative termination at $I = 62$. The band drawn for ^{152}Dy is the only superdeformed band in the $A = 150$ region whose absolute excitation energy is known [20]. Its interpretation is the same in different calculations based, for example, on the modified oscillator (CNS) [11,21], the Woods-Saxon potential [22], the Skyrme HFB [23], or the CRMF [24].

To extend the comparison of Fig. 1 to a larger mass region, we compare calculated and experimental energies for additional nuclei in Fig. 2, where different versions of the rotating liquid drop formula are used. The band observed to terminate at 8^{+} in ^{20}Ne [25] is built with two valence protons and two valence neutrons in orbits of $d_{5/2}$ character [26]. Cranked Nilsson-Strutinsky calculations on this band have been discussed, for example, in Ref. [27] and reviewed in [7]. The band in ^{36}Ar is the so-called superdeformed band, which is interpreted in CNS as well as shell-model calculations as having identical proton and neutron configurations with a total of four particles in orbits of $f_{7/2}$ character [28]. The additional bands included are the highest spin terminating states in ^{59}Cu [29] and ^{62}Zn [7,30], the SD band in ^{59}Cu [29], two more negative-parity bands in ^{156}Dy [19], and the SD band in ^{194}Hg [31]. These references are those where the bands have been discussed in the CNS formalism except for ^{194}Hg, which has not been described in this model previously but where we get the high-j $\pi(i_{13/2})^4\nu(j_{15/2})^4$ configuration in agreement with standard interpretation based on different models [32–34].

With the same parameters used in Fig. 1 and in the lower panel of Fig. 2, those data points that are repeated are identical. These parameters describe the data with good accuracy. Typical errors are in the range of ±1 MeV. Note especially that, from the data set considered here, the general trend as a function of mass number appears correct. This is contrary to the results in the upper panel, where in the static liquid drop energy, the LSD model has been replaced by the FRLDM. This results in systematic differences for light nuclei, where the calculated energies are lower than the experimental energies. Thus, the FRLDM predicts results similar to those

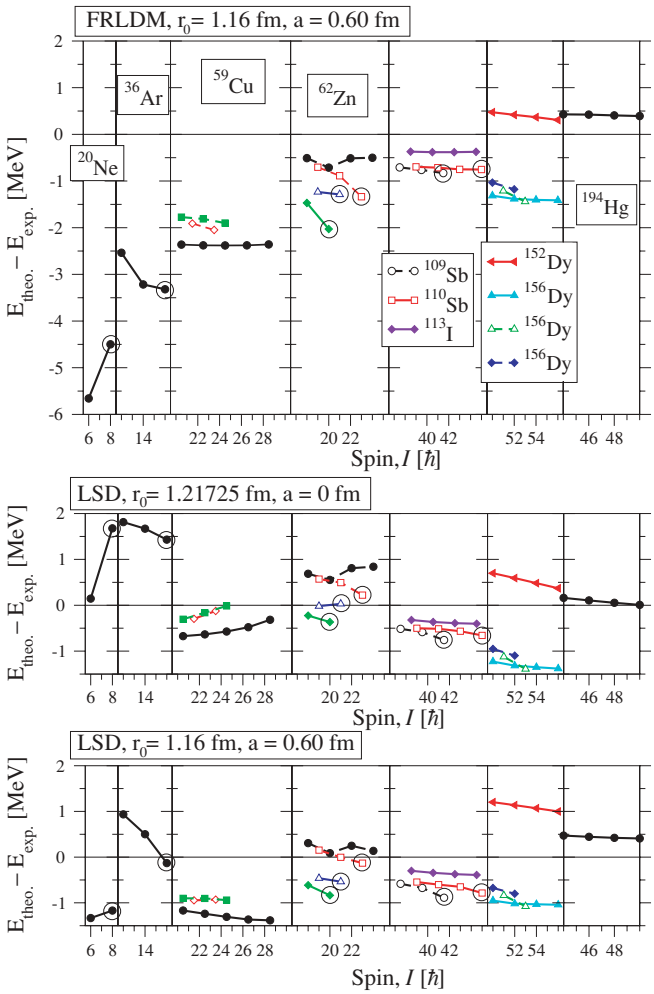

FIG. 2. (Color online) Difference in total energy between theory and experiment for the highest spin states of 10 nuclei with masses in the range A=20–194. In the lower panel, the same parameters as in Fig. 1 have been used whereas the FRLDM model has been used for the static liquid drop energy in the upper panel and the rigid moment of inertia has been calculated with a sharp surface in the middle panel.

of the LSD model for heavy nuclei but substantially lower total energies for ^{20}Ne, ^{36}Ar, and ^{59}Cu. One reason for this is that the two models are fitted to different shell corrections for $Z < 29$ and $N < 29$. Another reason is that for light nuclei the two models have different deformation dependencies, with the FRLDM being softer in the ε_2 and ε_4 directions. Therefore for light nuclei the FRLDM generally predicts somewhat larger ε_2 deformations and in some cases the ε_4 deformations are so large that the corresponding shapes appear unrealistic (cf. Ref. [35]).

The only difference between the two lower panels in Fig. 2 is that a sharp surface is used when calculating the rigid-body moment of inertia in the middle panel whereas a diffuse surface is used in the lower panel. The radius in the sharp-surface case is chosen as the value used to calculate the Coulomb energy in the LSD formula, $r_0 = 1.21725$ fm, corresponding to a rigid moment of inertia of a sphere, which is about the same as in the diffuse surface case for $A \approx 140$. In general, the differences

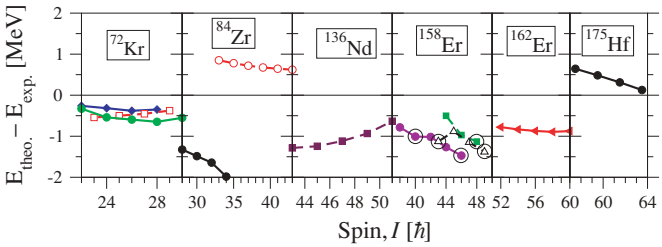

FIG. 3. (Color online) Same difference as in the lower panel of Fig. 2 for six additional nuclei in the mass range A=72–175.

between the two lower panels are not as great for heavy nuclei but become more pronounced for light nuclei. For example, the "diffuse moment of inertia" for spherical shape is around 13% bigger for $A = 36$ and more than 20% bigger for $A = 20$. Considering the trends in Fig. 2 and the physical understanding of the moment of inertia, we will from now on choose the LSD model for $E_{\rm ld}$ with $\mathcal{J}_{\rm rig.}$ calculated with a diffuse surface.

To get a wider selection, high-spin states of six more nuclei are considered in Fig. 3. They include the normal-deformed bands in the $N = Z$ nucleus ^{72}Kr and in ^{84}Zr, which have recently been extended to $I = 30$ [36] and to $I = 34$ [37], respectively, and the SD band in the latter nucleus, which has been connected [37] to the normal-deformed configurations. Calculations for the high-spin bands in ^{72}Kr using both the CNS and CRMF models are performed in Ref. [38] where it is found that both models give very similar results. The absolute spins of one band in ^{72}Kr are not known but the relative energies and comparisons with calculations strongly suggest the present interpretation [39]. The normal-deformed and superdeformed structures of ^{84}Zr have recently been discussed within the CNS [40] and the Woods-Saxon TRS approach [41], respectively. The respective configurations, which were also predicted [42] long ago, are identical to those used in Fig. 3. The band in ^{136}Nd [2] is a highly deformed triaxial band. For ^{158}Er a few more states are included than in Fig. 1, demonstrating that states of small or no collectivity are described with similar accuracy as collective states in our formalism. Finally, ^{162}Er [10] and ^{175}Hf [43] are the only deformed nuclei in the rare-earth region with collective bands observed up to $I = 60$. For the ^{175}Hf band, we calculate the same high-spin configuration as suggested in Ref. [43], $\pi(h_{9/2})^2\ (i_{13/2})^2\ \nu(i_{11/2})^2\ (j_{15/2})^1$.

As seen in Fig. 4, our selection of states covers a large region of the (ε_2, γ) plane, thus testing the mass model for a much wider selection of deformations than ground-state masses where mainly spherical and prolate deformations $(\gamma = 0)$ with $\varepsilon_2 \lesssim 0.3$ are relevant. A new feature is the large shape changes within specific bands so that different regions of deformation space are covered for one specific configuration. The importance of these deformation changes is illustrated, for example, in Fig. 30 of Ref. [7]. Indeed, from this figure one can conclude that if deformation changes were not properly taken care of, the difference curve for ^{109}Sb in the lower panel of Fig. 1 would look very different with fluctuations of the order of 1 MeV over a limited $(\Delta I < 10\hbar)$ spin range.

The new test of mass models introduced here could be compared with the calculation of fission barriers where the

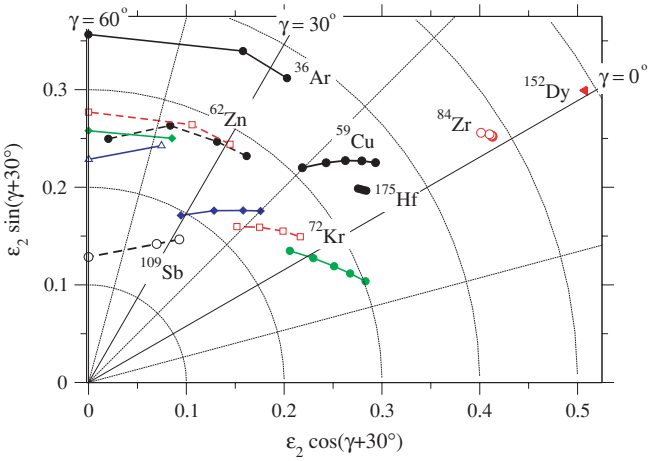

FIG. 4. (Color online) Calculated deformations of high-spin states for eight nuclei from Figs. 2 and 3, shown in the same spin interval as in those figures. Spin increases when going from right to left.

height of 28 barriers is commonly used to test the deformation dependence [5]. However, whereas the fission barrier test is mainly limited to heavy nuclei at large prolate deformation, there is no real limit on the possibilities of observing high-spin states at different deformations and comparing with calculations. Thus, especially for light nuclei, the study of the total nuclear energy at finite spin values will open new possibilities to perform systematic tests of different mass models and their deformation dependence. Of course, pairing and its decrease with angular momentum should then be included, making it possible to study the full (N, Z, I) space.

The rotational bands shown in Figs. 2 and 3 include most bands observed up into the unpaired regime and are rather evenly distributed over different mass numbers. The main omission are high-spin bands in the $A = 60$, $A = 110$, and $A = 155$–160 regions, but typical bands in these regions are already included and the additional bands would thus not add much information concerning the general agreement between calculations and experiment. Collective bands with $A > 160$ show the typical features of unpaired rotation only when approaching $I = 60$. Therefore we only consider such bands observed in this spin range, with the exception of the SD band of ^{194}Hg where pairing is probably of some importance even at the highest spins (see, for example, Refs. [33,34]).

For the 102 high-spin states included when using the LSD model, the rms value of the difference between calculated and experimental masses at high spin becomes 0.856 MeV. Considering that this agreement is obtained with no specific fit of parameters suggests that high-spin states can be described with the same or maybe even better accuracy than ground-state masses.

The fact that the absolute energy at fixed spin varies smoothly as a function of particle number (cf. [4]) makes it possible to get reliable estimates of spin values or to test tentative spin assignments. For example, if the spin values of the band shown for ^{110}Sb in Fig. 1 were wrong by $1\hbar$, it would show up as a difference between the ^{109}Sb and ^{110}Sb bands of more than 1 MeV in the lower panel (and also a

similar difference in the upper panel). Such discontinuities become much more accentuated at high spin where each unit of angular momentum corresponds to a much higher energy than for $I \approx 0$ [$E_\gamma(\Delta I = 1) \sim I/\mathcal{J}_{\text{rig.}}$]. Another advantage is that the absence of pairing at high spin makes it straightforward to compare odd, odd-odd, and even nuclei on the same scale. Note also that the position of single-particle orbitals could be tested from similar comparisons. For example, the comparison of the ^{109}Sb and ^{110}Sb bands is a direct test of the *single-particle* energy of the third $h_{11/2}$ neutron orbital as previously mentioned. Another interesting application is the calculation of particle decay energies at high spin values, which are easily obtained from the present formalism.

In summary, we have introduced an absolute energy scale for high-spin calculations and shown that the mass in the high-spin regime is well described using the CNS approach combined with the LSD model. This makes it possible to investigate systematic trends in the total energy at high spin, for example, comparing regions where the angular momentum is built mainly from collective rotation and mainly from single-particle excitations, respectively. Comparisons between neighboring nuclei makes it possible to test spin assignments and positions of specific single-particle orbitals.

The authors would like to thank Peter Möller for refitting the parameters of the FRLDM. They are grateful to Anatoli Afanasjev and Mark Riley for valuable comments on this manuscript. This work was supported by the Swedish Science Research Council.

[1] R. Bengtsson *et al*., Phys. Lett. **B105**, 5 (1981); in *Proceedings of the Nuclear Physics. Workshop, I.C.T.P., Trieste, Italy, Oct. 5–30, 1981*, edited by C. H. Dasso, R. A. Broglia and A. Winther (North Holland, Amsterdam, 1982), p. 273.
[2] S. Perriès *et al*., Phys. Rev. C **60**, 064313 (1999).
[3] I. Ragnarsson *et al*., Phys. Scr. **34**, 651 (1986).
[4] I. Ragnarsson *et al*., Int. J. Mod. Phys. **E13**, 87 (2004).
[5] P. Möller *et al*., At. Data Nucl. Data Tables **59**, 185 (1995).
[6] Z. Szymański, *Fast Nuclear Rotation* (Oxford University Press, Oxford 1983).
[7] A. V. Afanasjev *et al*., Phys. Rep. **322**, 1 (1999).
[8] T. Bengtsson and I. Ragnarsson, Nucl. Phys. **A436**, 14 (1985).
[9] W. Satula and R. A. Wyss, Rep. Prog. Phys. **68**, 131 (2005).
[10] J. Simpson *et al*., Phys. Rev. C **62**, 024321 (2000).
[11] T. Bengtsson, I. Ragnarsson, and S. Åberg, Phys. Lett. **B208**, 39 (1988).
[12] K. Pomorski and J. Dudek, Phys. Rev. C **67**, 044316 (2003).
[13] W. D. Myers and W. J. Swiatecki, Nucl. Phys. **A81**, 1 (1966).
[14] K. T. R. Davies and J. R. Nix, Phys. Rev. C **14**, 1977 (1976).
[15] H. De Vries, C. W. De Jager, and C. De Vries, At. Data Nucl. Data Tables **36**, 495 (1987).
[16] D. Vretenar *et al*., Phys. Rep. **409**, 101 (2005).
[17] K. Starosta *et al*., Phys. Rev. C **64**, 014304 (2001).
[18] J. Simpson *et al*., Phys. Lett. **B327**, 187 (1994).
[19] F. G. Kondev *et al*., Phys. Lett. **B437**, 35 (1998).
[20] T. Lauritsen *et al*., Phys. Rev. Lett. **89**, 282501 (2002).
[21] I. Ragnarsson, Nucl. Phys. **A557**, 167c (1993).
[22] W. Nazarewicz, R. Wyss, and A. Johnsson, Nucl. Phys. **A503**, 285 (1989).
[23] P. Bonche, H. Flocard, and P. H. Heenen, Nucl. Phys. **A598**, 169 (1996).
[24] A. V. Afanasjev, G. A. Lalazissis, and P. Ring, Nucl. Phys. **A634**, 395 (1998).
[25] T. K. Alexander *et al*., Nucl. Phys. **A179**, 477 (1972).
[26] A. Bohr and B. R. Mottelson, *Nuclear Structure*, Vol. 2 (Benjamin, New York, 1975), p. 96.
[27] I. Ragnarsson, S. Åberg, and R. K. Sheline, Phys. Scr. **24**, 215 (1981).
[28] C. E. Svensson *et al*., Phys. Rev. Lett. **85**, 2693 (2000).
[29] C. Andreoiu *et al*., Eur. Phys. J. A **14**, 317 (2002).
[30] C. E. Svensson *et al*., Phys. Rev. Lett. **80**, 2558 (1998).
[31] T. L. Khoo *et al*., Phys. Rev. Lett. **76**, 1583 (1996).
[32] M. A. Riley *et al*., Nucl. Phys. **A512**, 178 (1990).
[33] B. Gall *et al*., Z. Phys. A **348**, 183 (1994).
[34] A. V. Afanasjev, P. Ring, and J. König, Nucl. Phys. **A676**, 196 (2000).
[35] L.-O. Jönsson, Nucl. Phys. **A608**, 1 (1996).
[36] C. Andreoiu *et al*., Phys. Scr. **T125**, 127 (2006).
[37] C. J. Chiara *et al*., Phys. Rev. C **73**, 021301(R) (2006).
[38] A. V. Afanasjev and S. Frauendorf, Phys. Rev. C **71**, 064318 (2005).
[39] B. G. Carlsson and I. Ragnarsson, Phys. Scr. **T125**, 130 (2006).
[40] R. Cardona *et al*., Phys. Rev. C **68**, 024303 (2003).
[41] F. Lerma *et al*., Phys. Rev. C **67**, 044310 (2003).
[42] I. Ragnarsson and T. Bengtsson, in *Proceedings of the International Workshop, on Nuclear Structure of the Zirconium Region, Bad Honnef, April 1988*, edited by J. Eberth, R. A. Meyer, and K. Sistemich (Springer-Verlag, Berlin, 1988) p. 193.
[43] D. T. Scholes *et al*., Phys. Rev. C **70**, 054314 (2004).